Available online at www.sciencedirect.com
ScienceDirect
Acta Materialia 58 (2010) 3493–3503
Acta MATERIALIA
www.elsevier.com/locate/actamat

Kinetics of dislocations in pure Fe. Part I. In situ straining experiments at room temperature

D. Caillard *

CEMES-CNRS, 29 rue J. Marvig, BP 4347, 31055 Toulouse Cedex, France

Received 26 January 2010; received in revised form 5 February 2010; accepted 11 February 2010
Available online 11 March 2010

Abstract

In situ straining experiments have been carried out in pure Fe, in order to determine the geometry and the kinetics of dislocation glide at room temperature. Straight screw dislocations glide slowly in {1 1 0} elemental slip planes, at a velocity proportional to their length, whereas curved non-screw parts are highly mobile. The exact loop shape can yield the local stress as well as the difference of core energy between pure screw and near-screw orientations. The velocity–stress dependence of screws has been measured at the scale of a single dislocation source, and compared with macroscopic activation areas. The results are discussed in terms of the kink-pair mechanism.

Keywords: Iron; Dislocation mobility; Plastic deformation; Thermally activated processes

1. Introduction

The low-temperature mechanical properties of body centred cubic (bcc) metals exhibit all the characteristic features of strongly thermally activated mechanisms, in particular a strong increase of flow stress at decreasing temperature, and small activation areas. Such behaviour is typical of very short-range interactions between moving dislocations and rate-controlling obstacles. It is especially favourable to the study of fundamental dislocation properties, because the flow stress is in principle directly related to the mobility of individual dislocations, which itself is determined by elementary mechanisms operating at the atomic scale.

Concerning bcc metals, it is well known that their plastic deformation is controlled by the motion of screw dislocations, in a periodic potential originating from their non-planar core structure. The mechanical properties of bcc metals have been extensively studied by several groups, whose main results are summarized in review papers by Kubin [1], Christian [2], Suzuki et al. [3], Duesberry [4], Taylor [5], and Caillard and Martin [6]. At the atomistic scale, great strides have been made recently in the description of dislocation core structures under stress, by Duesberry and Vitek [7], Domain and Monnet [8], Chaussidon et al. [9], Ventelon and Willaime [10], Gröger et al. [11–13], Clouet et al. [14], and Ventelon [15]. However, the complete link between the mechanical properties and the dislocation core structure remains difficult to establish. In particular, the following points remain unsolved:

(i) What is the exact elementary slip plane of screw dislocations? Is it {1 1 0}, according to recent atomistic calculations yielding non-degenerate compact cores, or {1 1 2}, in agreement with previous conclusions based on the existence of two types of degenerate cores? Is there a change of elementary slip plane at 200–250 K, as postulated by Brunner and Diehl in Fe [16]?
(ii) What is the origin of the discontinuity observed in the temperature dependence of the activation area of several bcc metals? In Fe, this discontinuity has been observed at 200–250 K by Quenel et al. [17], Kuramoto et al. [18], Aono et al. [19], and Brunner and

* Tel.: +33 5 62 25 78 72; fax: +33 5 62 25 79 99.
E-mail address: caillard@cemes.fr

1359-6454/$36.00
doi:10.1016/j.actamat.2010.02.023

Diehl [20]. Is it due to a specific shape of the Peierls potential profile, as suggested by Takeuchi [21], Aono et al. [19], and Koizumi et al. [22]? Does it result from a change of kink-nucleation plane, as proposed by Brunner and Diehl [16]? Or is it due to another change of dislocation mechanism [6]?

(iii) Which explanation could be proposed for the large difference between the Peierls stress deduced from atomistic calculations, and the flow stress extrapolated to 0 K? Is it due to pile-up effects, as suggested recently by Gröger and Vitek [23], or to some unexpected softening mechanism at low temperature?

(iv) Is it possible to find simple explanations for the various effects of interstitial and substitutional alloying elements? For instance, what could be the origin of the complex effect of carbon atoms in iron, i.e. hardening below 150 K, and softening between 150 K and 250 K (see e.g. Ref. [18])?

Answers to these questions require a good knowledge of the dynamic properties of dislocations, which can be deduced from in situ observations. Several in situ experiments were carried out in the 1970s, in Fe and Fe alloys, by Furubayashi [24], Kubin and Louchet [25], and in Nb by Ikeno and Furubayashi [26], and Louchet et al. [27]. However, the resolution of the high-voltage electron microscopes used at that time was too poor to reveal all the details of the dislocation glide mechanism. The aim of this study is thus to re-investigate the dynamic properties of dislocations in Fe and Fe alloys, at various temperatures, and as a function of stress. Elements of response to the above questions will be proposed in this study. In this first part, the properties of dislocations in pure Fe are investigated at room temperature, and described in terms of the kink-pair mechanism. In the subsequent article (part II), their evolution upon decreasing the temperature to 100 K will be related to points (i–iii) above. The effects of some alloying elements will be analysed and related to point (iv) in separate articles.

2. Experimental procedure

A large-grain polycrystal of pure iron was provided by J. Le Coze, Ecole des Mines of St. Etienne, France. The amount of residual C, N, O, and Si atoms was 2.5–4 ppm-wt (ppm in weight), 15 ppm-wt as a whole, and the amount of other elements was less than 2 ppm-wt. The initial density of dislocations was rather low, of the order of 10^7 cm^{-2}. Rectangles of size 3 mm × 1 mm, thickness 50 μm were cut by spark erosion, mechanically polished, and electrochemically polished to perforation at their centre. They were glued on a GATAN room temperature straining holder, and observed in a JEOL 2010 HC transmission electron microscope, using a Megaview III video camera operating at 25 images per second. The microsamples were deformed in the microscope by series of constant strain-rate deformations and relaxations, at an average strain-rate of 10^{-6}–10^{-5} s^{-1}. All results were obtained in a grain of plane normal $[\bar{1}\,2\,3]$, and straining direction $[1\,\bar{4}\,3]$. The images were taken with the diffraction vector [2 2 0], at a tilt angle of −8°.

As discussed in Ref. [28], the stress is concentrated and the deformation starts in the two zones where the average tensile axis is tangential to the thin-edged hole. Since the corresponding local stress direction is close to the global straining one, the operating slip systems can be predicted by the Schmid law (with all restrictions inherent to the bcc structure), except in front of crack tips where the stress distribution is more complex. Possible thin foil artefacts will be discussed in several situations where they may be important.

To analyse the motion of dislocations, the intensities of two superimposed images were subtracted: as a result the background and the immobile dislocations vanish, but moving dislocations appear in positive (former position) and negative (new position) contrasts. Rapidly moving dislocations exhibit fuzzy images, of width equal to their displacement during the exposure time. Under such conditions, a homogeneous fuzzy contrast denotes a constant velocity, whereas a discontinuous contrast denotes a varying instantaneous velocity [29]. The method to deduce the local stress from the curvature of dislocations will be described in Section 3.2.

3. Results

The grain investigated deforms by the motion of dislocations with Burgers vector $b = \frac{1}{2}[\bar{1}\,\bar{1}\,1]$, making an angle of 42° with the global (and presumably local) straining axis.

The most interesting measurements have been made at sources, where all dislocation characters can be observed simultaneously, far enough from the free surfaces to avoid possible thin foil artefacts.

3.1. Description of a source emitting cross-slipping dislocations

Fig. 1 shows one revolution of a single-ended source pinned in *S*. The dislocation exhibits straight screw parts, and curved non-screw ones. The screw part moves slowly to the left, till it meets the anchoring point P, at $t = 0.56$ s (Fig. 1c). It subsequently moves further till the curved non-screw part reaches its critical position, at $t = 2.32$ s (Fig. 1d). This curved part then escapes suddenly to the top, between $t = 2.32$ s and $t = 2.36$ s (Fig. 1e), leaving a dipole of two opposite screw segments. The velocity of the free non-screw part, between $t = 2.32$ s and $t = 2.36$ s, is several orders of magnitude higher than that of the neighbouring screw segments. It cannot be measured with the time resolution of the video camera. It is important to note that the motion of the dislocation arc PS between $t = 0.56$ s and $t = 2.32$ s is not influenced by the free surfaces according to the rules established in Ref. [28]. Then, the left screw segment disappears to the left side, whereas the right one moves to the right until another critical non-screw part is ready to escape to the bottom ($t = 4.32$ s, Fig. 1g). When emerging at the top

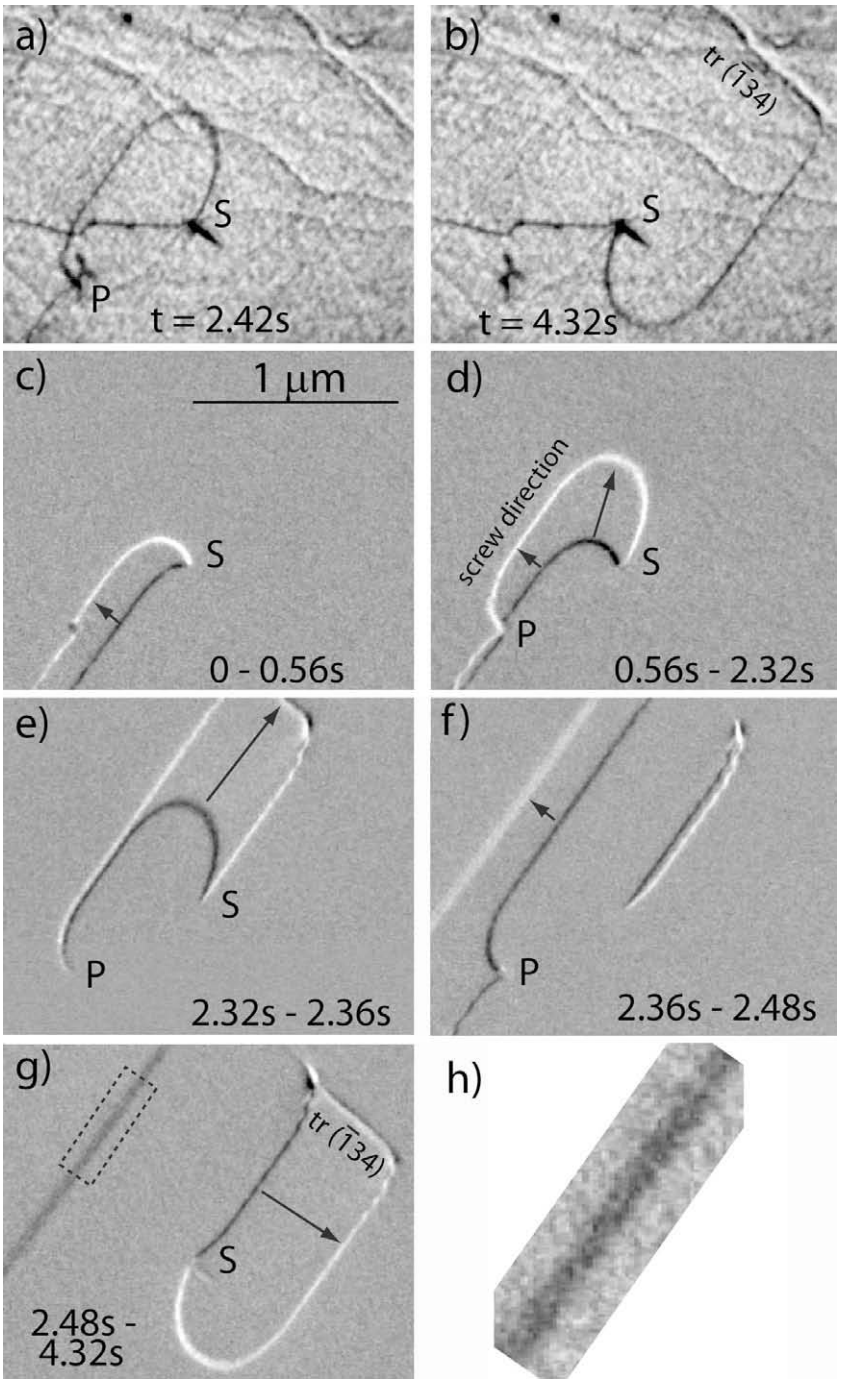

Fig. 1. Dislocation source rotating around the anchoring point *S*. Two different positions of the rotating dislocation are shown, in (a) and (b), and successive difference-images are shown in (c–g). The trace at one sample surface indicates slip in the average ($\bar{1}$ 3 4) plane. Note the slow motion of the two opposite straight screw segments, the fast motion of the non-screw part, in (e), and the pinning, in *P*. The fuzzy contrast of the dislocation emitted to the left in (g), is enlarged in (h). See video as Supplementary material.

free surface, the loop leaves a wavy trace, noted tr. The corresponding slip surface is thus non-planar, as a result of intensive cross-slip. The average slip plane, namely the plane containing the average trace direction and the Burgers vector, is close to ($\bar{1}$ 3 4) in this case. It can be noted that the velocities of the two opposite screw segments are very different between $t = 2.36$ s and $t = 2.48$ s (Fig. 1f). This can be deduced from the different displacement distances, but also from the fuzzier contrast of the most rapid dislocation [29]. The fuzzy contrast (enlarged from (g) in (h), and discussed in Section 2) is fairly regular, which indicates a constant velocity during the exposure time (of the order of 1/50 s). The origin of these different dislocation velocities will be discussed in Section 3.3.

Fig. 2 shows the slip traces left by 10 successive revolutions of the source at the upper foil surface. They are all

wavy, and correspond to average slip planes ranging between $(\bar{1}\,1\,0)$ and $(0\,1\,1)$. Several slip surfaces are close to the $(\bar{1}\,2\,1)$ plane. All slip traces approximately converge at a single point, noted C, because slip surfaces must contain the screw direction going through the rotation axis *S*. Unfortunately, the elemental glide planes at the atomic scale cannot be determined in this sequence. They will be determined at another source described in Section 3.4.

3.2. Loop shape, and core energy of screw segments

Figs. 3 and 4 correspond to two different rotations of the source described above, in two different average slip planes. The perspective effects have been corrected by enlarging the images along the directions perpendicular to the intersections between the respective average slip planes and the observation plane (these intersection directions being close to the trace directions). Then, corrected images have been compared with those calculated with the software DISDI provided by Douin [30]. Using anisotropic elastic constants, this software computes the dislocation line energy and line tension, and determines the equilibrium loop shape in a given glide plane, as a function of the shear stress.

Fig. 3 shows the dislocation loop gliding in a $(\bar{1}\,2\,1)$ average plane, whereas Fig. 4 shows the same loop gliding subsequently in an average plane close to $(0\,1\,1)$. The slightly non-symmetrical shape in $(0\,1\,1)$ arises from the fact that $\{1\,1\,0\}$ planes are not symmetrical with respect to the $\langle 1\,1\,1\rangle$ direction of the Burgers vector. In particular, it can be noted that the dislocation curved in $(0\,1\,1)$ exhibits a cusp noted C, at the top-left side, which corresponds to a local minimum of the line tension, and which is well reproduced in the simulation. Such a good fit between experiment and simulation shows that non-screw parts have reached their equilibrium position, namely that they are subjected to a negligible friction stress. Under such conditions, the loop size can yield the exact local shear stress. In the above examples, the best fit is obtained for a local shear stress $\tau = 33$ MPa.

It can also be noted that experimental dislocation shapes deviate from theoretical ones at the vicinity of the screw orientation. As shown in Ref. [31], this occurs because the elastic calculation is based on a fixed core energy, whereas the real core energy is lower in the pure screw orientation. The departure point (arrowed) is rather difficult to localize accurately, but the careful examination of Figs. 3b and c and 4b and c indicates that it occurs at $\theta \sim 27°$,

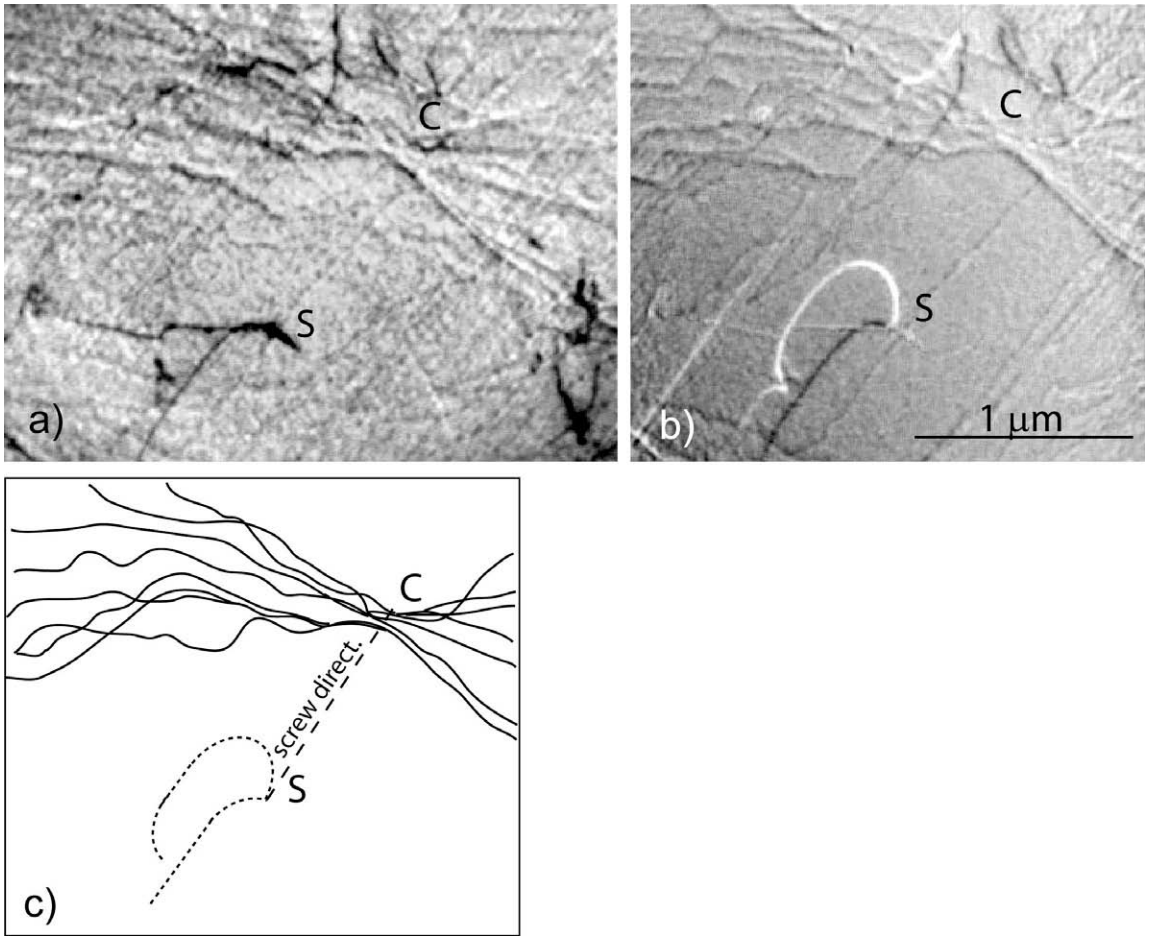

Fig. 2. Wavy slip traces left by the source of Fig. 1. (a) is a bright-field image, (b) is the difference between two bright-field images separated by several rotations of the source, (c) is the corresponding scheme. Note the convergence of all traces at C, emergence point of screw dislocations going through *S*.

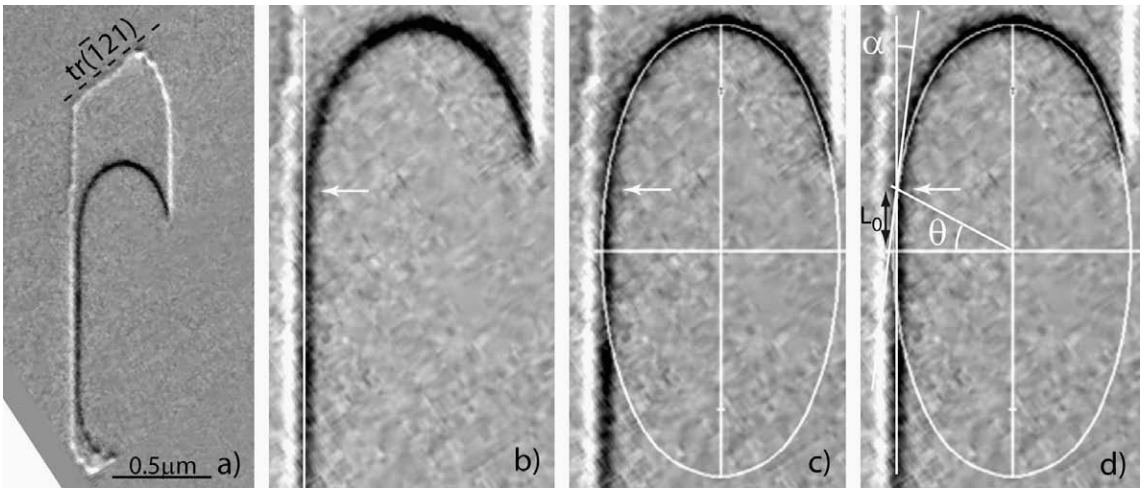

Fig. 3. Loop shape in a {1 1 2} plane (deduced from the corresponding average slip trace). The screw direction is vertical. The dark and bright contrasts correspond to two successive positions of the same dislocation. The curved loop (in dark) is compared with its theoretical shape, calculated using anisotropic elasticity constants, under a stress of 33 MPa. The departure point where the curved near-screw part straightens is arrowed, and the corresponding change of dislocation direction is noted α.

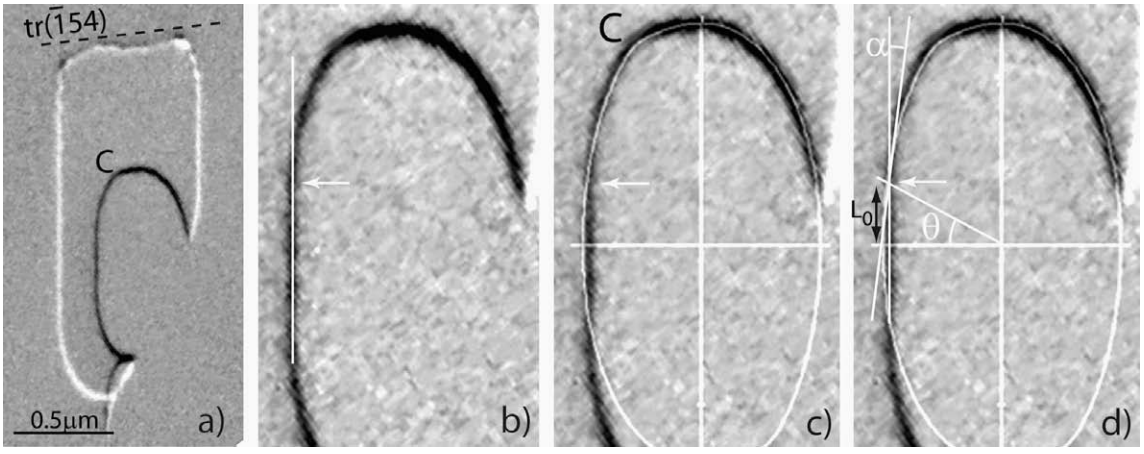

Fig. 4. Loop shape in a plane close to {0 1 1} (same notations as in Fig. 3). Note the cusp corresponding to a sharp minimum of line tension, in C.

which corresponds to a change of dislocation direction $\alpha = 7° \pm 1°$. The screw length introduced by this straightening effect, L_0, will be shown to be consistent with further results in Section 3.3.

The change of dislocation direction is abrupt, which indicates that there is no pile-up of kinks at screw extremities (compare Fig. 5a and b). If E is the total dislocation line energy close to the screw direction, the decrease of core energy between near-screw and pure screw segments, ΔE, can be estimated using the relation given in Ref. [31], which, for small values of α, reduces to $\Delta E/E = \alpha^2[(1/2) + \nu/(1-\nu)]$. With $\nu = 0.29$, and $\alpha = 7° \pm 1°$, we obtain $10^{-2} < \Delta E/E < 1.77 \times 10^{-2}$. Taking $E = 1.75 \times 10^{-9}$ J m^{-1} = 2.7 eV per Burgers vector length (from the software DISDI [30]), this corresponds to $\Delta E \sim 37$ meV/b (27 meV/b $< \Delta E <$ 48 meV/b). This value is consistent with the depth of Peierls valleys deduced from ab initio calculations (ΔE = 28–40 meV b, according to Ref. [15]).

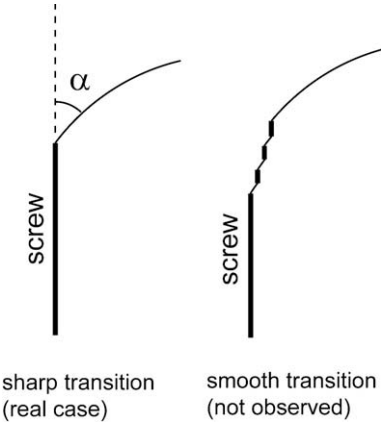

Fig. 5. Schematic description of a sharp and a smooth transition, between the screw and near-screw parts of a dislocation loop.

3.3. Length effect

The different velocities of the two opposite screw dislocations in Fig. 1 arise from their different lengths, as shown in Fig. 6. The successive positions of the right screw segment (during a revolution different from that shown in Fig. 1) have been imaged at constant time intervals of 0.4 s and 0.2 s. The dislocation is pinned at its lower extremity, at the source anchoring point S. It is also curved at its upper extremity at the free surface, because it trails a slip trace which costs some energy. Note that this curvature ensures that there is no kink-nucleation at the free surface, namely that the glide process should be correctly reproduced in the thin foil. The velocity first decreases, and then increases, which can be correlated to the variation of length of the straight screw part, L. To determine L with the highest possible accuracy, the images have been processed as in Figs. 3 and 4, and the two curved extremities have been fitted with the corresponding theoretical profiles. Then, the screw length has been considered to be $L = L_1 + 2L_0$, where L_1 is the distance between the two half profiles, and L_0 is the length determined in Figs. 3 and 4. Fig. 6 shows that L_1 first decreases, for $\theta < \pi/2$, and then increases, for $\theta > \pi/2$.

The average dislocation velocity between two successive images of Fig. 6 has been plotted in Fig. 7 as a function of the average length L of the starting and final positions. The variation is linear and goes through the origin, which confirms that the determination of L_0 in Section 3.2 is correct. This length effect is similar to that already observed in magnesium [32] and in several semi-conducting compounds [33]. It will be discussed in Section 4.

3.4. Determination of the elementary slip planes of screw dislocations

The elementary slip planes could not be determined in the above situations where cross-slip is too frequent. The discrimination between the two candidates {1 1 0} and {1 1 2} type planes is thus possible only where the local stress favours repeated elementary glide processes in the same plane.

Fig. 8 exhibits many straight slip traces corresponding to the almost edge-on $(\bar{2}\,1\,\bar{1})$ planes (Schmid factor 0.48), which could be interpreted as a preference for this type of plane. However, the close inspection of the source anchored in S clearly shows that the occurrence of this {1 1 2} slip is a thin foil artefact. Different successive positions of the rotating dislocation (same $\frac{1}{2}[\bar{1}\,\bar{1}\,1]$ Burgers vector as in the above observations) are shown in the left column, and noted a, b, ..., e, whereas the corresponding difference-images are shown in the right column, and noted

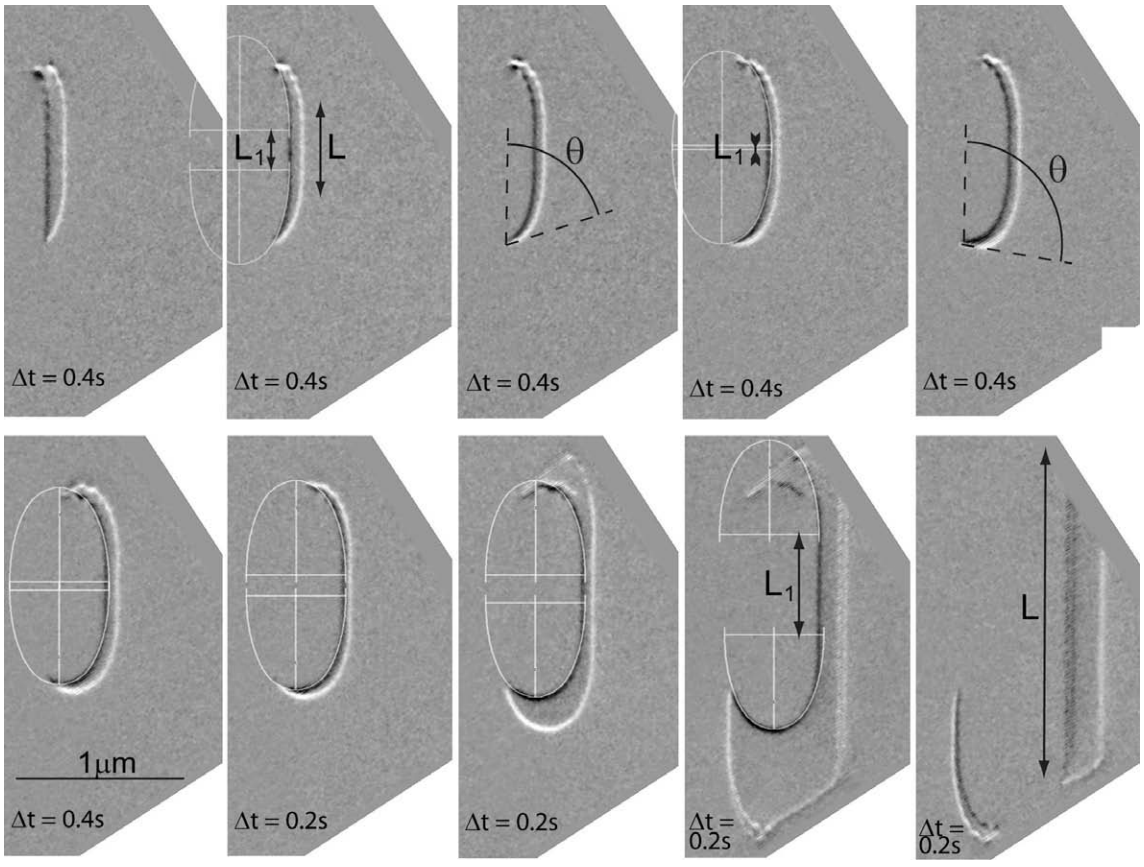

Fig. 6. Successive positions of a dislocation loop, first every $\Delta t = 0.4$ s, and then every $\Delta t = 0.2$ s. L_1 is the distance between two half profiles, and L is the total length in the pure screw orientation (vertical). The stress is considered to remain constant during the short duration of the sequence.

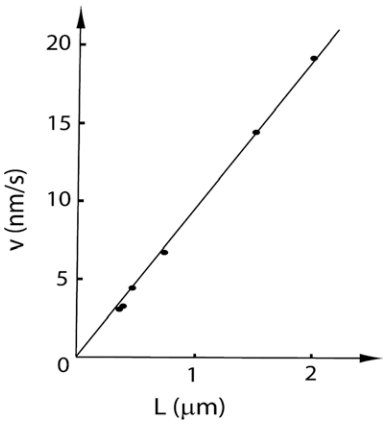

Fig. 7. Velocity of pure screw segments, as a function of their length. Data from Fig. 6.

a and b, b and c, ..., d and e (the last difference-image, noted a–e, illustrates the total motion between a and e). These images show that the source rotates in the $(\bar{1}\,1\,0)$ plane (Schmid factor 0.48), which is more inclined with respect to the thin foil than $(\bar{2}\,1\,\bar{1})$. However, as shown in Fig. 9, the emitted screw dislocations can considerably reduce their length (and so their total energy) when they emerge at the two surfaces, by rotating to the [0 1 1] edge direction nearly perpendicular to the foil plane. Since this occurs via a cross-slip into the edge-on $(\bar{2}\,1\,\bar{1})$ plane, the near-edge dislocations are stabilized in the $(\bar{2}\,1\,\bar{1})$ plane where they can glide freely. This kind of cross-slip is probably initiated at the two surfaces, which is clearly a thin foil artefact. On the contrary, the source operation in the $(\bar{1}\,1\,0)$ plane, close to the anchoring point S, should not be influenced by the free surfaces. This demonstrates that, in a situation where the $(\bar{1}\,1\,0)$ and $(\bar{2}\,1\,\bar{1})$ planes have the same Schmid factor, but where the $(\bar{2}\,1\,\bar{1})$ plane is favoured by the sample geometry, dislocation multiplication, which requires the motion of all dislocation characters including the screw one, can take place only in $(\bar{1}\,1\,0)$. In other words, edge dislocations can glide in either $(\bar{1}\,1\,0)$ or $(\bar{2}\,1\,\bar{1})$, but the motion of screw ones is confined in $(\bar{1}\,1\,0)$. More generally, no stable glide of screw dislocations has been observed in {1 1 2} planes. The elemental slip planes involved in the wavy motion of screw dislocations are thus unambiguously of the {1 1 0} type.

3.5. Activation area for single dislocations

Discontinuous straining with long relaxation periods induces important changes of dislocation velocity, which can be correlated with substantial variations of the local stress. For each rotation of the source of Fig. 1, the local stress has been determined by the method used in Section 3.2. According to Section 3.3, the dislocation velocity must be measured at a constant length. In a first step, the variation of the dislocation length has been assumed to be the same for all rotations of the source, and the average velocity has been deduced from the duration of each revolution. The corresponding variation of dislocation velocity with stress has the slope $n_1 = \Delta \ln v / \Delta \ln \tau \approx 4.9$ (Fig. 10). However, this procedure may introduce a systematic error, because the length of pure screw segments slightly decreases when the radius of curvature of the non-screw parts increases, namely when the stress decreases. The dislocation velocity has thus been plotted as a function of the real dislocation length, measured as in Fig. 6, for several rotations of the source. The slope of the corresponding velocity per unit length, as a function of stress, is then $n_2 = \Delta \ln(v/L)/\Delta \ln \tau \approx 2.7$ (Fig. 10). It is substantially lower than the preceding one, which indicates that the variation of the average length with stress cannot be neglected.

Another similar measurement is shown in Fig. 11. Fig. 11a corresponds to Fig. 8d and e, whereas Fig. 11b has been extracted from the rotation of another source, with the same geometry, but in a thicker part of the sample. The two difference-images appear similar in shape and size, except that: (i) the scale bars are in a ratio of two (which means that the stress is approximately twice higher in (a)), and (ii) the velocity of the screw dislocation is the largest in (a) (see the fuzzy contrast due to the displacement during the exposure time). A precise determination of the loop size (Section 3.2) yields $\tau_a = 50$ MPa and $\tau_b = 25$ MPa. In (b), the screw of length L_b has moved over the distance x_b during one frame (1/25 s), whereas in (a), the screw of length L_a has moved over the distance x_a (the width of the fuzzy contrast) during the exposure time ($\approx$1/50 s). The corresponding ratio of the velocities per unit length is thus $(v_a/L_a)/(v_b/L_b) = 8.3$. This yields the stress–velocity dependence $n_3 = \Delta \ln(v/L)/\Delta \ln \tau \approx 3$, in a good agreement with the value n_2 determined above.

The corresponding activation areas, $A = nkT/\tau_b$, are respectively $A_2 = 23b^2$ and $A_3 = 21b^2$. They have the same order of magnitude as the macroscopic values deduced from conventional mechanical tests (e.g. $A = 55b^2$ at 300 K, according to Ref. [20]).

4. Discussion

The steady motion of rectilinear screw dislocations is typical of the kink-pair mechanism, for which the velocity can be expressed as

$$v = v_D \frac{bLh}{x_c^2} \exp - \frac{U_{kp}(\tau)}{kT} \tag{1}$$

where U_{kp} is the energy of a kink-pair at its saddle position, under the local shear stress τ, v_D is the Debye frequency, x_c is the critical length for nucleating a kink-pair, $v_D b/x_c$ is the order of magnitude of the dislocation vibration frequency, of wave length x_c, and L/x_c is the number of nucleation sites for the dislocation length L.

For sufficiently large kink separations at the saddle position (kink separation larger than the kink-width), the kink–kink interaction is of Coulomb-type. Then, the activation energy can be written as [6,34]

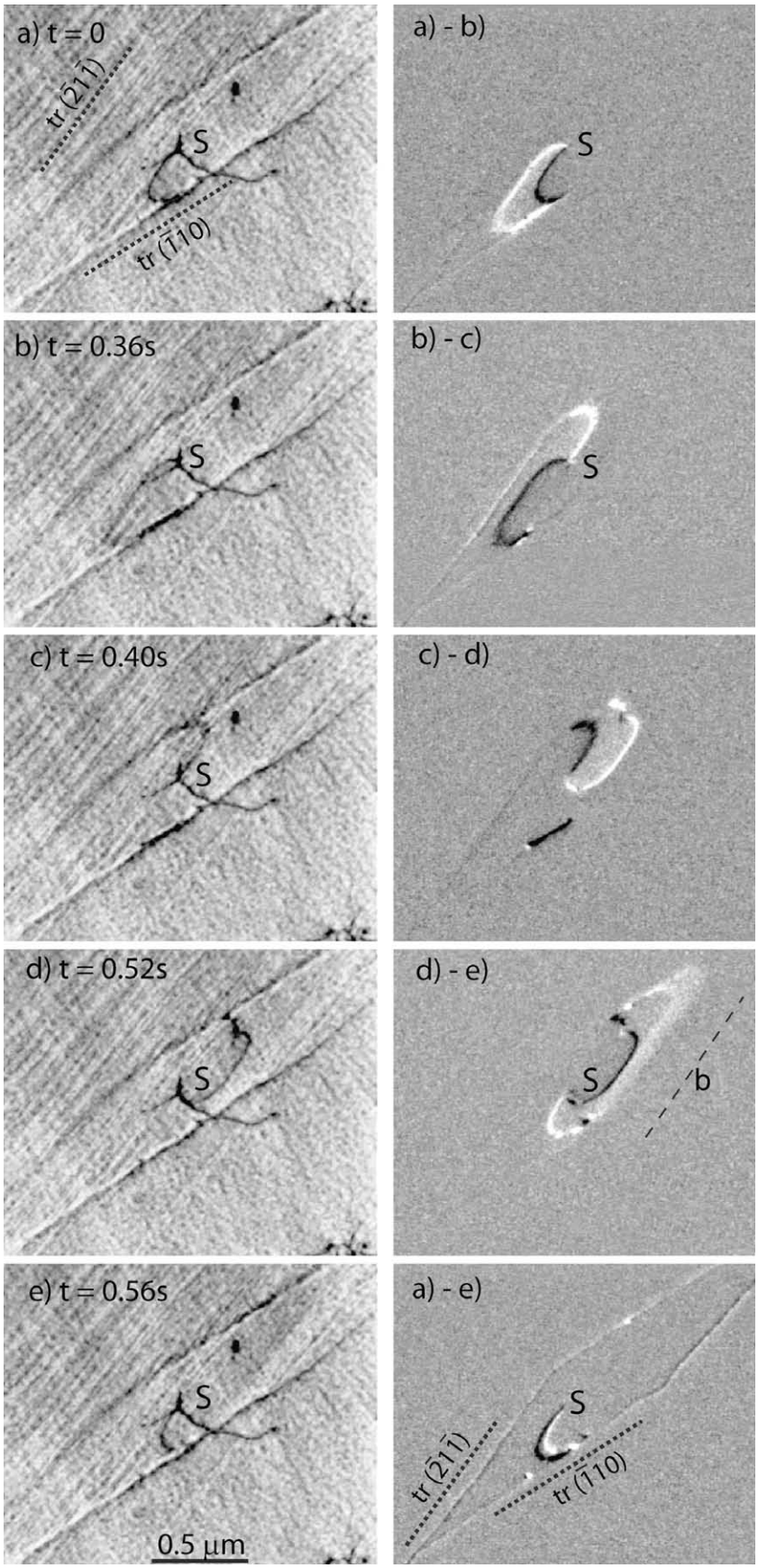

Fig. 8. Dislocation source rotating in the ($\bar{1}$ 1 0) plane, around the anchoring point *S*. The Burgers vector direction is *b*. As soon as the emitted screw segments emerge at the foil surfaces, they cross-slip in the ($\bar{2}$ 1 $\bar{1}$) plane in order to reduce their length. The whole process is schematically described in Fig. 9 (see text). See video as Supplementary material.

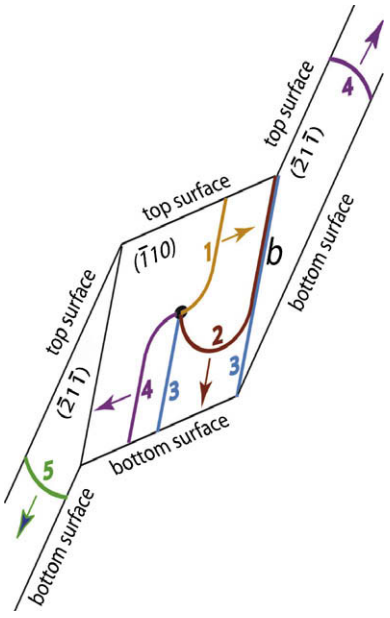

Fig. 9. Schematic description of the source of Fig. 8. The source operates in the (1̄ 1 0) plane, but the dislocations cross-slip in the edge-on (2̄ 1 1̄) plane when they emerge at the surfaces.

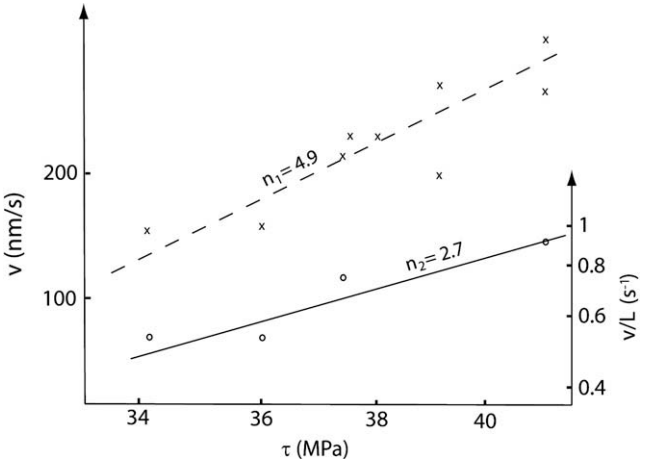

Fig. 10. Stress dependence of the velocity of a single screw dislocation. The slope n_1 is deduced from the duration of each rotation of the source, whereas n_2 is deduced from the dislocation velocity per unit length, v/L.

$$U_{kp} = 2U_k - (hb)^{3/2}\left(\frac{\mu\tau}{2\pi}\right)^{1/2} \quad (2)$$

where U_k is the energy of an isolated kink, and μ is the shear modulus.

The velocity v is considered to be proportional to the dislocation length L, because each kink issued from a pair is assumed to glide to the dislocation extremity, i.e. the time between two successive kink-pair nucleations is assumed to be longer than the time for kink propagation along the dislocation line. This proportionality has been verified experimentally (Fig. 7), which confirms that the kink velocity is very high.

The probability of cross-slip is so high that dislocations can glide in any average glide plane, depending on the local stress direction. This is in a fairly good agreement with the slip line observations carried out at the same temperature, reviewed in Ref. [4]. However, the observations in Section 3.4 clearly show that the elemental slip planes of screw dislocations are of the {1 1 0} type. This result agrees with the most recent atomistic calculations, showing that screw dislocations have non-degenerate cores, and move by kink-pair nucleation in {1 1 0} planes [15]. It is however at variance from the conclusion of Brunner and Diehl [20] that kink-pairs nucleate in {1 1 2} planes at room temperature. One possible explanation for this discrepancy will be proposed below.

The microscopic activation area, $A_{micro} = kT\Delta \ln v/b\Delta\tau$, has been deduced from the variation of the dislocation velocity per unit length with local stress. Its most plausible value is $A_{micro} \approx 22b^2$, for an average local stress $\tau = 37$ MPa. This value is smaller than that measured in conventional mechanical tests at the same temperature but at a lower stress ($A_{macro} = kT\Delta \ln \dot{\varepsilon}/b\Delta\tau \approx 50b^2$, for $\tau = 20$ MPa, from Brunner and Diehl [16]). Part of this difference may be attributed to the different deformation stresses. However, the larger value of A_{macro} also probably arises from the decrease of the mobile dislocation density with decreasing stress, observed during in situ relaxation tests. As a matter of fact, the relation $\Delta \ln \dot{\varepsilon}/\Delta\tau = \Delta \ln \rho/\Delta\tau + \Delta \ln v/\Delta\tau$ (where ρ is the mobile dislocation density) shows that $A_{macro} > A_{micro}$, provided $\Delta \ln \rho/\Delta\tau > 0$. The same difference has been found in magnesium, and has also been attributed to the decrease of the mobile dislocation density with decreasing stress [32].

The experimental value A_{micro} is now compared with theoretical ones. Assuming that Eq. (2) is valid, the activation area should be

$$\frac{A_{th}}{b^2} = \left(\frac{h}{b}\right)^{3/2}\left(\frac{\mu}{8\pi\tau}\right)^{1/2} \quad (3)$$

With $h = (2\sqrt{2}/3)b$ (which corresponds to glide in {1 1 0} planes), $\tau \approx 37$ MPa, and $\mu = 115$ GPa, this theoretical value is $A_{th} = 10b^2$, i.e. substantially lower than the experimental one ($A_{micro} \approx 22b^2$). One reason for this discrepancy is that for such low values of the activation area, the kink separation at the saddle position ($x_c \approx 20$b) is equivalent to the kink-width (of the order of $10b$, according to atomistic calculations [15]). Then, the simplifying assumption of a Coulomb interaction, at the origin of Eqs. (2) and (3), is not valid at 300 K.

The differences between A_{micro}, A_{macro}, and A_{th}, may explain why Brunner and Diehl [16] concluded that the plane of kink-pair nucleation is {1 1 2}, instead of {1 1 0}. Indeed, these authors deduced the kink height h from the comparison between their experimental activation areas and Eqs. (2) and (3). Since they assumed that: (i) the dislocation density remains constant during relaxations tests (namely $A_{micro} = A_{macro}$), and (ii) Eq. (3) is valid (namely $A_{micro} = A_{th}$), it is natural that they overestimated h, which

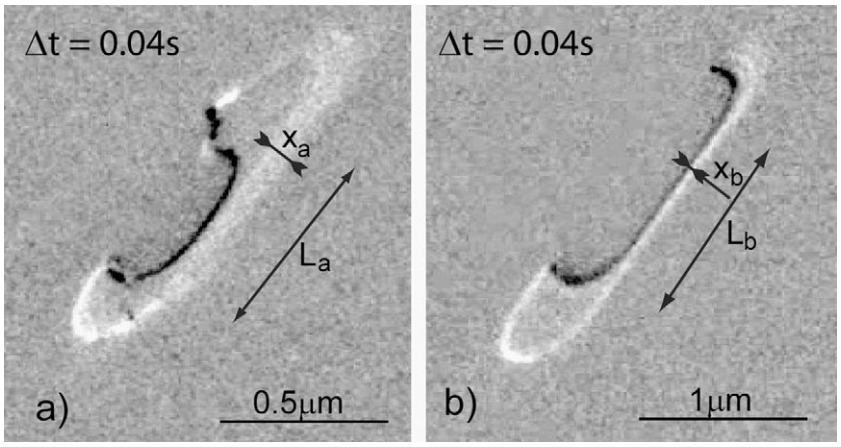

Fig. 11. Comparison between the velocities of two screw dislocations, of length L_a, in (a), and L_b, in (b). x_a and x_b are the displacements respectively during the exposure time, in (a), and between two frames, in (b). Note the similar shapes, but different scales, showing that the local stress is twice higher in (b) than in (a).

was then too large to fit with kink-pair nucleation in {1 1 0}. On the contrary, it appears that h cannot be deduced directly from activation area measurements, even when A_{micro} is known, because the assumption of a Coulomb kink–kink elastic interaction is no more valid at 300 K and below.

5. Conclusions

In situ straining experiments in pure Fe at room temperature have shown that:

- Dislocation loops exhibit straight screw segments moving slowly and steadily, and much more highly mobile non-screw parts.
- The curvature of non-screw parts is determined by the equilibrium between their line tension and the local stress. This shows that the friction stress on all non-screw orientations is negligible. The local stress can accordingly be deduced from the loop size ($\tau \sim 33$ MPa, close to the macroscopic value of the critical resolved shear stress).
- Screw and near-screw parts make an angle of about 7° at their junction point, which allows one to estimate the corresponding difference of core energy ($\Delta E \sim 37$ meV/b, close to the depth of Peierls valleys).
- The velocity of screws is proportional to their length.
- The elemental slip planes have been determined in spite of extensive cross-slip. They are of the {1 1 0} type.
- A microscopic activation area has been measured on a single dislocation. It is $23b^2$, slightly lower than the macroscopic one.
- All the results are consistent with a kink-pair mechanism, where the critical kink separation is too short to be described by a Coulomb-type elastic interaction.

Acknowledgments

The author warmly thanks Jean Le Coze (Ecole des Mines St. Etienne) for the elaboration of the iron ingot, Dominique Lamirault and Jacques Crestou for the preparation of microsamples, and Prof. Jacques Friedel (Orsay University) for his very stimulating comments. This work has been supported by the European Fusion Development Agreement.

Appendix A. Supplementary material

Supplementary data associated with this article can be found, in the online version, at doi:10.1016/j.actamat.2010.02.023.

References

[1] Kubin L. In: Feltham P, editor. Reviews on the deformation behaviour of materials, vol. 4(3). Tel Aviv (Israël): Scientific Pub. Div. Freund Pub. House Ltd.; 1982. p. 181.
[2] Christian JW. Met Trans 1983;14A:1237.
[3] Suzuki T, Takeuchi S, Yoshinaga Y. Dislocation dynamics and plasticity, vol. 12. Berlin: Springer Series in Materials Science, Springer-Verlag; 1985.
[4] Duesberry MS. In: Nabarro FRN, editor. Dislocations in solids, vol. 8. North Holland, Amsterdam; 1989. p. 67.
[5] Taylor G. Prog Mater Sci 1992;36:29.
[6] Caillard D, Martin JL. In: Cahn RW, editor. Thermally activated mechanisms in crystal plasticity. Amsterdam: Pergamon materials series; 2003.
[7] Duesberry MS, Vitek V. Acta Mater 1998;46:1481.
[8] Domain C, Monnet G. Phys Rev Lett 2005;95:215506.
[9] Chaussidon J, Fivel M, Rodney D. Acta Mater 2006;54:3407.
[10] Ventelon L, Willaime F. J Comput-aided Mater Des 2007;14:85.
[11] Gröger R, Bailey AG, Vitek V. Acta Mater 2008;56:5401.
[12] Gröger R, Racherla V, Bassani JL Vitek V. Acta Mater 2008;56:5412.
[13] Gröger R, Vitek V. Acta Mater 2008;56:5426.
[14] Clouet E, Ventelon L, Willaime F. Phys Rev Lett 2009;102:055502.
[15] Ventelon L. Ph.D. Université Claude Bernard, Lyon; 17 November 2008.
[16] Brunner D, Diehl J. Phys Stat Sol(a) 1991;125:203.
[17] Quenel DJ, Sato A, Meshii M. Mater Sci Eng 1975;18:199.
[18] Kuramoto E, Aono Y, Kitajima K. Scripta Met 1979;13:1039.
[19] Aono Y, Kitajima K, Kuramoto E. Scripta Met 1981;15:275.
[20] Brunner D, Diehl J. Phys Stat Sol(a) 1997;160:355.
[21] Takeuchi S. Philos Mag A 1979;39:661.

[22] Koizumi H, Kirschner HO K, Suzuki T. Acta Met Mater 1993;41:3483.
[23] Gröger R, Vitek V. Philos Mag Lett 2007;87:113.
[24] Furubayashi E. J Phys Soc Jpn 1969;27:130.
[25] Kubin LP, Louchet F. Acta Met 1979;27:337.
[26] Ikeno S, Furubayashi E. Phys Stat Sol(a) 1975;27:581.
[27] Louchet F, Kubin LP, Vesely D. Philos Mag A 1979;39:433.
[28] Couret A, Crestou J, Farenc S, Molenat G, Clement N, Coujou A, Caillard D. Microsc Microanal Microstruct 1993;4:153.
[29] Caillard D. Philos Mag Lett 2009;89:517.
[30] Douin J, Veyssière P, Beaucham P. Philos Mag A 1986;54:375.
[31] Douin J, Castany P, Pettinari-Sturmel F, Coujou A. Acta Mater 2009;57:466.
[32] Couret A, Caillard D. Acta Metall 1985;33:1455.
[33] Louchet F, Pelissier J, Caillard D, Peyrade JP, Levade C, Vanderschaeve G. Microsc Microanal Microstruct 1993;4:199.
[34] Eshelby JD. Proc Roy Soc Lond 1962;A266:222.